Biosensors and Bioelectronics 66 (2015) 497–503

Contents lists available at ScienceDirect

Biosensors and Bioelectronics

journal homepage: www.elsevier.com/locate/bios

Gold nanostar based biosensor detects epigenetic alterations on promoter of real cells

Anh H. Nguyen, Xingyi Ma, Sang Jun Sim*

Department of Chemical and Biological Engineering, Korea University, Seoul 136-713, Korea

ARTICLE INFO

Article history:
Received 20 October 2014
Received in revised form
2 December 2014
Accepted 3 December 2014
Available online 5 December 2014

Keywords:
Plasmonic biosensors
Gold nanostars
DNA methylation
Peptide nucleic acid
Plasmon coupling
Epigenetics

ABSTRACT

Epigenetic changes, particularly in cancer suppressor genes, are novel biomarkers for cancer diagnostics and therapeutics. However, epigenetic studies should not only provide an estimation of the amount of 5-methylcytosine, but also examine the presence of epigenetic proteins to reveal the complete epigenetic alterations for downstream molecular process. The challenge of natural epigenetics is to unveil key factors of epigenetics in one assay, containing low concentrations. This would be valuable for the monitoring of early-stage cancer. On the basic of the nanoplasmonic biosensor, here we report a sensitive sensor to study epigenetics of DNA promoter. The results show detection limit for dual epigenetic biomarkers methyl-CpG group and methyl-CpG binding domain protein 2 (MBD2) are one 5-methylcytosine molecule and 125 fM MBD2. Moreover, DNA structure bending, steric competition under interaction of epigenetic proteins and transcription factors; and epigenetics-mediated suppression of transcription are observed during epigenetic alterations. This study provides a platform for full story of epigenetics, as compared with that of methylcytosine-based techniques only.

© 2014 Elsevier B.V. All rights reserved.

1. Introduction

Nanoplasmonics-based refractometric platforms are facilitating end-point and kinetic monitoring as next-generation novel biosensors because of their extreme sensitivity to changes of the active refractive index (RI), inside the surface plasmon decay length (δ_d) (Brolo, 2012). The sensors bring together two exceptional features. The first is high sensitivity in end-point detection, which can be determined at very low concentrations. The second is monitoring of the biological phenomena in δ_d of plasmonic nanoparticles (Song et al., 2013). Localized surface plasmon resonance (LSPR) is a coherent oscillation of the surface conduction electrons excited by electromagnetic radiation at a nanoscale, which strongly depends on the RI sensitivity of the nanoparticles, changes in RI, δ_d, and binding thickness. Moreover, plasmons of gold nanoparticles, which are collective oscillations of their conduction electrons, do not blink or photobleach, in contrast to fluorescent dye molecules (Sonnichsen et al., 2005; Reinhard et al., 2005). The plasmon due to coupling mode is sensitive to the vicinity between the particles in a distance-dependent manner (Reinhard et al., 2007). The resonant plasmon wavelength can be red-shifted from blue regions into infrared regions due to a reduction in the inter-particle distance. In particular, the LSPR transducer response is very sensitive to changes closer to the surface, which is required for the measurement of biomolecular kinetics.

Epigenetic changes play important roles in abnormal activation and silencing of genes that have been associated with cancer (Egger et al., 2004), chromosomal instability-linked syndromes (Robertson, 2002) and mental retardation (Penagarikano et al., 2007). Recent reports demonstrated sensor-based detection of methylation on single stranded DNA (ssDNA) (Wang et al., 2012; Hu and Zhang., 2012; Stains et al., 2006). However, real epigenetic change is a process that occurs on methylated double stranded (dsDNA), with the participation of epigenetic proteins directly influencing the transcription of a gene, in particular, in the promoter regions. Previous reports revealed that peptide nucleic acid (PNA) molecules hybridize and form stable complexes with dsDNA (Nielsen et al., 1991; De et al., 2013; Nguyen and Sim, 2014). Therefore, using PNA molecules to capture dsDNA is an applicable approach to then examine the number of 5-methylcytosine (methyl-CpG) sites, and to unveil epigenetics.

Here, we present a nanoplasmonic biosensor which was fabricated using PNA-functionalized gold nanostars (AuNSs) for epigenetic study of the p53 promoter. The sensor demonstrated the following results: a limit of detection of one methyl-CpG and 125 fM MBD2 for real measurement of epigenetic interactions; evidence of the bending of p53 structure and steric competition under interaction of transcription factors and epigenetic proteins; lower transcription of the epigenetically-mediated transcription of the p53 promoter. These results allowed to measure dual complementary

* Corresponding author: Fax: +82 2 926 6102.
E-mail address: simsj@korea.ac.kr (S.J. Sim).

http://dx.doi.org/10.1016/j.bios.2014.12.015
0956-5663/© 2014 Elsevier B.V. All rights reserved.

biomarkers at low concentrations, eliminates the necessity of chemical modifications, and permits direct monitoring of the epigenetics on a specific gene as pivotal biomarkers for the early stages of epigenetics-driven cancer. The sensor can also be applied to the monitoring of drug development for epigenetic therapeutics, diagnostics for epigenetic changes of circulating tumor DNA.

2. Materials and methods

2.1. End-point detection for intimately associated dual biomarkers of epigenetics

Fabrication of the sensor was described in the supplementary method S2 (see Supplementary materials). A hybridization buffer (perfectHyb^{TM}, Sigma) containing the p53 promoters (300 ng) was injected into the fabricated biosensor chamber and incubated for 2 h at 52 °C, pH 5.4, to form a stable complex. The PNA probes complementarily hybridized to methylated p53, following the Watson–Crick Model (Nielsen et al., 1991). The temperature was set at 52 °C and pH at 5.4 to achieve optimal hybridization and minimize nonspecific binding (Supplementary Fig. S1). The temperature was then raised to 64 °C and the NaCl concentration was set to 100 mM to eliminate nonspecific binding. The conjugation of PNA on OEG_6COOH-functionalized AuNSs via EDC/NHS coupling was verified using FT-IR spectroscopy, and electrophoresis confirmed the presence of PNA-p53 promoter complexes on the AuNSs (Supplementary Fig. S2). For estimation of the detection limit of the LSPR-peak shift, a range of recombinant MBD2 concentrations (125×10^{-6} fM to 125×10^{6} fM) (New England Biolabs) were used. A range of methyl-CpG sites (1–4 sites) on the p53 promoter was used to measure the saturation of LSPR-peak shift. To check for nonspecific binding, the specificity was challenged corresponding with two characteristics: specificity for the p53 promoter, and specificity for methyl-CpG binding. For the p53 promoter, its PNA probes were used with several DNA sequences (Supplementary Table S1); for methyl-CpG binding, MeCP2, lysosome and p53 proteins were incubated with the mp53 promoter under the same conditions.

2.2. Characterization of bending of the methylated p53 promoter and MBD2-mediated steric competition

Plasmonic coupling was applied to measure the bending of the p53 promoters under epigenetic conditions. 213 bp forward strands (F) (100 nM) and 213 bp reverse strands (100 nM) of the p53 promoter (R) with methylation (mp53 promoter) and without methylation (p53 promoter) were bound with 45-nm AuNSs. After immobilization of F-AuNSs, the R-AuNSs were injected into the chamber and incubated in hybridization buffer. The inter-particle distance was about 72.4 nm (213 bp, 3.4 nm for 10 bp), which is outside the plasmon band (Brolo, 2012). 200 µl of HeLa nuclear extracts (HeLaScribe®, Promega) were injected into the chamber and incubated at 37 °C for 1 h. Bending of the p53 promoters induced by transcription factors was monitored in the plasmonic coupling mode, based on inter-particle distance, plasmon-coupled mode occurring as collective excitation between the nanoparticles. The adsorption and coupling mode phenomena were different from the peak shape of the LSPR spectra (Reinhard, et al., 2005).

In the experiment for MBD2-mediated steric competition, 300 ng PNA probes capturing methylated fragments transcription binding sites and 125 fM MBD2 were injected into the biosensor chamber, and then incubated for 2 h at 37 °C. 100 pM of each of the TFs was subsequently injected and incubated for 2 more hours. To determine the steric competition, the LSPR values of each binding were recorded. The binding to the surface after each step was washed by using the regeneration buffer (pH 5.4/ PBS 0.01% SDS solution). To check MBD2 saturation on the sensor surface, the surface was treated with 100 pM of anti-MBD2 antibody after incubation with MBD2.

2.3. Epigenetics-based suppression of transcription

The sensor was used to identify epigenetics-mediated transcription of the mp53, p53, He-p53, and Hk-p53 promoters. The p53 promoter sequences contained 243 nucleotides, including the region of promoter basic activity (213 bp) and an extended part of exon 1 (from +1 to+30) for the transcription. The status of genomic methylation of HeLa and HEK293 cell lines was examined by Imprint® Methylated DNA Quantification (Sigma-Aldrich) (Supplementary Fig. S3A). The nuclear extracts were divided into two parts, with the MBD2 molecules in the second part eliminated (e.MBD2) by an anti-MBD2 antibody affinity column (Supplementary Fig. S3B). For measuring epigenetics-mediated transcription, two conditions were measured: (i) MBD2-free conditions and (ii) MBD2-dependent conditions. In (i), the p53 promoters on the sensor surface were overlaid with 200 µl of MBD2-free HeLa nuclear extracts (190 µl HeLa nuclear extract in 1 × transcription buffer, 10 µl 25 mM $MgCl_2$) and incubated for 2 min before the addition of 1x ribonucleotides mixture (0.4 mM rATP, 0.4 mM rCTP, 0.4 mM rUTP, 16 µM rGTP) in 1 × transcription buffer. When the ribonucleotide solution reached the sensor, the LSPR spectra were immediately measured with exposure time 0.2 s at 40 °C. For MBD2-dependent measurements, the same procedure was conducted in the presence of MBD2 molecules. The transcription reaction was stopped after 20 min, and the RNA products in the solution were alternatively measured with a Qubit RNA assay kit (Invitrogen, USA) and a spectrofluorophotometer (Shimadzu, Japan).

3. Results and discussion

3.1. Sensor fabrication and data analysis

The sensor was fabricated based on the refractive index sensitivity of AuNSs. The plasmon resonances of AuNSs were reported extreme sensitive to the local dielectric environment at single structure compared with that of other shapes (Rodríguez–Lorenzo et al., 2012; Nehl et al., 2006). For sensor fabrication (Fig. 1A), AuNSs (45 nm) were synthesized from a surfactant-stabilized seed (Nehl et al., 2006) (Fig. 2A), immobilized on a glass support, and functionalized with PNA as the bioreceptor. Each AuNS plays the role of a biosensor element. AuNSs were functionalized with PNA to catch the region of basic promoter activity of p53 promoter (NCBI J04238), for identification of methylation on a 213-bp sequence, and to analyze the native p53 basic promoter activity region, for revealing epigenetics. First, binding of MBD2 into the methyl-CpG sites was assessed and subsequent analysis of the steric competition between MBD2 and transcription factors was performed by measuring the LSPR-peak shift due to RI changes. Second, the stiffness of mp53 promoters was monitored by analyzing the structural bending of the p53 promoter with an *in vitro* transcription system (HeLaScribe®, Promega). Bending of the structure due to the transcription factors was detected by plasmon coupling mode between two nanoparticles on the sensor platform (Fig. 1A (ii and iii)). Plasmon shift of a coupled pair of dimers depends on the inter-particle distance in the nuclear extract medium (RI 1.6) (Sonnichsen et al., 2005; Reinhard et al., 2005). Third, epigenetically-mediated suppression of transcription was monitored by measurement of the changes of local RI in real time, within δd (Fig. 1A (i) (green arrow)). Dark-field microscope showed plasmon scattering in end-point detection, DNA stiffness and epigenetics-mediated transcription (Fig. 1B).

The plasmon shifts are dependent on the binding affinity and rate constant of human RNA polymerase II (RNAP II) with the p53 promoter, which was captured on the surface of the AuNSs (Fig. 1A (i)). The relative promoter activity was determined by the changes to LSPR λ_{max} due to RNAP II binding, moving closer proximity to the AuNSs. Transcriptional activity of a promoter, V, is described by how efficiently an RNAP II synthesizes RNA, and is given by the following equation (Browning et al., 2009; Tsunoda and Takagi, 1999): $V=k_t$. K (1).

Where k_t is the rate constant of transcription, and K is the binding affinity. The rate constant, k_t, is a numerical benchmark of the overall transcription process, including the binding of RNAP II, formation of the pre-initiation complex, initiation, elongation, and termination phases. The velocity of RNAP II moving along DNA is about 35–80 nucleotides per s (Besmer et al., 2006). Real-time transcription was monitored with exposure time 0.2 s. The number of methyl-CpGs on the p53 promoter not only reduced the binding rate of RNAP II, but also disturbed formation of the initiation complex formation, as well as elongation and termination (Pogribny et al., 2000; Ng et al., 1999). Therefore, the rate-determining step for the promoter activity, V, is the binding of RNAP II to the promoter (Kugel and Goodrich, 1998). Since LSPR λ_{max} is proportional to the RNAP II activity on the promoter, which was bound to the surface of the biosensor, the relative mp53 promoter activity is determined by the following equation:

$$v_r \approx \frac{k_{bm}\ \Delta\lambda_{\max,m}}{k_{b,um}\ \Delta\lambda_{\max,um}} \quad (1)$$

Where ν_r is the relative activity of the mp53 promoter; $k_{b,m}$ and $k_{b,um}$ are the rate constants of RNAP II binding to the mp53 and p53 promoters, respectively; and $\Delta\lambda_{max,\ m}$ and $\Delta\lambda_{max,\ um}$ are the LSPR λ_{max} shifts generated from the translocation of RNAP II closer to the AuNS surface, along with the mp53 and p53 sequences, respectively.

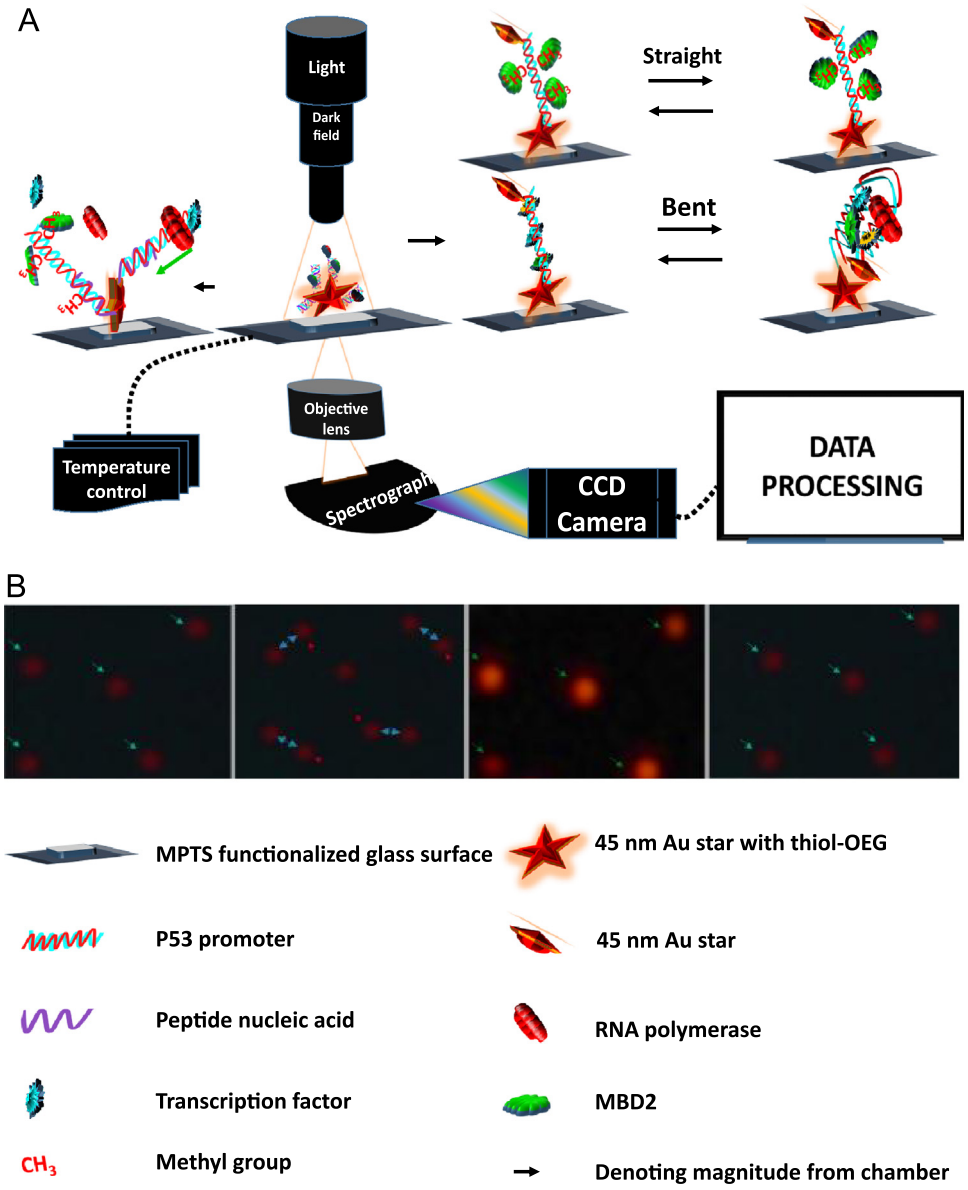

Fig. 1. Sensor fabrication. (A) Schematic showing the overall sensor fabrication for multiple applications: (i) Refractometric endpoint detection and epigenetics-mediated. transcription; (ii, iii) plasmon coupling-based. measurement of p53 promoter bending. (B) Dark-field. of sensor with surface binding and plasmon coupling. Individual sensors for end-point. detection are visible as red dots (cyan arrows). In case of methylated p53 promoter, straight form upon stiffness shows ~72-nm dimer association (3.4 nm/10 bp of 213 bp) (two-headed. arrows and red arrows). Dimer dissociation upon bending leads to enhance intensities of plasmonic scattering. Distinct dimers are converted into coupling monomers as shown for selected particles (green arrows). Bending structure of p53 promoters is monitored in the nuclear extract of HeLa cell. (For interpretation of the references to color in this figure legend, the reader is referred to the web version of this article.)

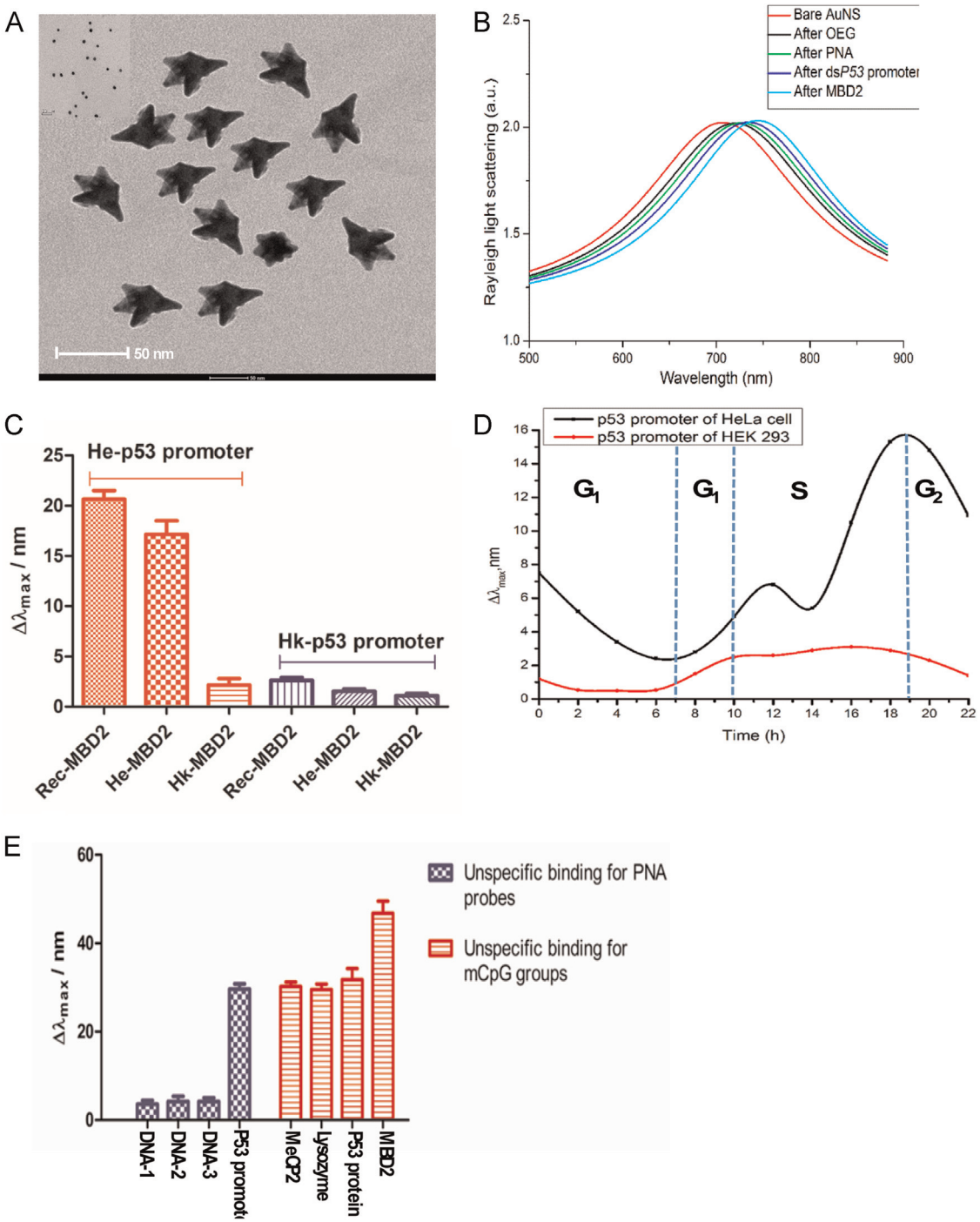

Fig. 2. Methyl-CpG and MBD2 detection. (A) TEM image of gold nanostars and their surfactant-stabilized seeds (left corner) (diamater of AuNS $d_1 = 45$ nm, diamter of AuNPs $d_2 = 12$ nm). (B) LSPR-peak shift of detecting one methyl-CpG group on p53 promoter and 125 fM MBD2. LSPR shift 18.3 nm from bare AuNS to OEG functionalization step, 4.9 nm from OEG to PNA step, 6.3 nm from PNA to p53 promoter hybridization, 12.3 nm for after MBD2 binding. (**C**) $\Delta\lambda_{max}$ (nm) values reflect proportional relationship between methylation of p53 promoter and MBD2 concentration. HeLa p53 promoters are treated with MBD2 from recombinant rec-MBD.2 (20.5 nm), He-MBD.2 (16.2 nm) and Hk-MBD.2 (2.4 nm). Similarly, HEK 293 p53 promoter are treated with MBD2 from rec-MBD.2 (2.6 nm), He-MBD.2 (2.3 nm) and Hk-MBD.2 (2.2 nm). (D) Dynamics of p53 promoter methylation of HeLa (black line) and HEK (red line) cells in cell cycles. $\Delta\lambda_{max}$ (nm) values as function of the cell cycle time (h). (E) Unspecific detection for p53 promoters and MBD2 targets. Unspecific molecules were challenged for the biosensor at PNA hybridization step (DNA-1,-2,-3) and mCpG recognition step (MeCP2, lysozyme and p53 protein). The error bars in (C) and (E) represent s.d calculated from three times measured at each promoter. The scale bar in (A) and inlet are 50 nm and 20 nm, respectively. (For interpretation of the references to color in this figure legend, the reader is referred to the web version of this article.)

3.2. *End-point detection for intimately associated dual biomarkers of epigenetics*

It was previously shown that MBD2 specifically binds into methyl-CpG sites without surrounding A/T sequences, for example, in the p53 promoter (Klose et al., 2005). The number of methyl-CpG sites was measured by analyzing the LSPR-peak shift after MBD2 binding. Fig. 2A and Supplementary Fig. S4A demonstrates that the limit of detection of the sensor was one methyl-CpG site and 125 fM of MBD2, corresponding to a 12.3 nm shift in the LSPR-peak, from 29.5 nm after PNA hybridization with mp53 to 41.8 nm after MBD2 binding to the single methyl-CpG site. The shift in the LSPR-peak at

varying MBD2 concentrations and methyl-CpG-dependentLSPR-peak shift saturation are shown in Supplementary Fig. S4B. The LSPR-peak shift ranged from 0.5 nm to 23.6 nm as MBD2 concentrations increased from 125×10^{-6}–125×10^{6} fM. This demonstrates that one-step label-free biosensing exhibits much higher sensitivity and simpler detection than the current methods (Wang et al., 2012; Hu and Zhang, 2012), even of dual biomarkers: DNA methylation status, and MBD2 concentration. We found mp53 and p53 promoters to have similar affinities with the PNA probes (supplementary Fig. S2). The PNA probes were then used to capture the p53 promoter from digested gDNA of different cell lines. Efficient recovery of PNA receptors was achieved by increasing the temperature to 64 °C to denature the hydrogen bond between PNA and the p53 promoters, which did not interfere with the quality of PNA for continued use.

To determine the epigenetic changes in real samples, the methylation of p53 promoters and MBD2 concentrations in HeLa and HEK293 cell lines were examined. Methylation of the p53 promoter and high concentrations of MBD2 are the characteristics of these cells (Oshiro et al., 2003). To examine the promoters from real test cells, 243-bp fragments of the promoters were extracted from the cell line genomes using XbaI and BamHI, and were enriched in the binding chamber. To examine the native epigenetic proteins, nuclear extracts were obtained from the cell lines. LSPR-peak shifts ($\Delta\lambda_{max}$) occurred at 21.5 nm, 15.9 nm, and 2.9 nm when the HeLa p53 promoter (He-p53) was incubated with recombinant MBD2 (rec. MBD2), HeLa nuclear extracts (He-MBD2), and HEK293 nuclear extracts (Hk-MBD2), respectively, compared with PNA-dsp53 conjugated AuNS. However, an LSPR-peak shift was not observed when the HEK293 p53 promoters (Hk-p53) were incubated with recombinant MBD2 (rec. MBD2), HeLa nuclear extracts (He-MBD2), and HEK293 nuclear extracts (Hk-MBD2), respectively (Fig. 2C). As the shift in the LSPR peak depends on the number of methyl-CpGs in the p53 promoter and the concentration of MBD2 in the samples, these results reflected that the methylation status and MBD2 concentrations in HeLa cells are higher than those in HEK293 cells regarding the epigenetics of p53. These results also demonstrated that the dual biomarkers provided a significant biomarker for the analysis of epigenetics-driven cancers.

We also employed the sensor to test whether epigenetic changes in the p53 promoter are static or dynamic during the cell cycle. HeLa and HEK 293 cells, as well-known models for cell cycle analysis, were chosen for this analysis (Brown et al., 2007). $\Delta\lambda_{max}$ (Fig. 2D) showed that epigenetic changes occur at different phases of the cell cycle. Dynamic epigenetic changes were proportional to the dynamic methylation and expression of MBD2 of the cell lines. Compared with previous reports (Wang et al., 2012; Hu and Zhang, 2012; Zhang et al., 2014; Shim et al., 2012), using the sensor to monitor dynamic epigenetics provided more sensitive, informative and comprehensive results, as there is a native interaction between methyl-CpG and MBD2. In HeLa cells, dynamic epigenetic changes were observed from G_1 to G_2, with a decreasing during G_1 phase for 8 days, after which they increased in the S phase. In HEK 293 cells, however, only low levels of changes were observed. $\Delta\lambda_{max}$ increased from 7.5 nm to 15.3 nm for HeLa cells, but only from 0.49 nm to 3.1 nm for HEK 293 cells in the hyper methylated state. These results demonstrated the epigenetic changes to the p53 promoter during the cell cycle, particularly in cancer cells.

3.3. Stiffness of methylated P53 promoter and MBD2-mediated steric competition

We measured the conformational changes of the p53 promoter using plasmon coupling mode on the sensor platform. Plasmon coupling mode occurs when gold nanoparticles stay at small enough distances, and the plasmonic resonances are very sensitive to inter-particle gaps (Ringe et al., 2012; Reinhard et al., 2007; Lange et al., 2012). Plasmon coupling disappears for inter-particle gap more than 70 nm ($d = 70$ nm) apart, but occurs strongly at short distances ($d < 30$ nm), in the plasmon band of the particles (Brolo, 2012; Lange et al., 2012).

Transcriptional activation induces promoter bending to regulate gene transcription (Kuznetsov et al., 2006). Transcription factors bind loosely to normal promoter structures, then causing the structure to bend in order to form the transcription initiation complex (Jolma et al., 2013). In the mp53 promoter (Fig. 3A), however, MBD2 and other epigenetic proteins bind into the methyl-CpG sites, hindering the binding of transcription factors and strengthening the stiffness of the mp53 promoter (Deaton and Bird, 2011). Fig. 3B shows plasmon coupling mode of p53 promoter bending, which is fitted with the Lorentz algorithm. During activity of the transcription factors, bending of the p53 promoter generated a 110 nm shift in the LSPR peak due to plasmon coupling (blue curve). The red curve represents an 11.5 nm RI-based red shift due to the binding of MBD2 with mp53. The results from plasmonic coupling demonstrated that mp53 is less flexible, causing inhibition of the dynamic interaction with transcription factors, which is a vital mechanism to facilitate the transcription process (Kuznetsov et al., 2006; Jolma et al., 2013).

Analysis of the steric competition between MBD2 and transcription factors (TFs) may reveal biological roles in the suppression of p53 transcription. Using the sensor to clarify this interaction could uncover the mechanism of formation of the pre-initiation complex, without the need of chemical modification. The LSPR-peak shift was first recorded at 16.6 nm after incubation with MBD2. To monitor the interaction, 100 nM of TFs including AP-1, NF-κB, YY1, and c-Myc, were injected into the chamber containing mp53-MBD2 complexes. However, no shifts in the LSPR spectra were observed (Fig. 3C and supplementary Fig. S5). Conversely, an LSPR-peak shift was recorded at 9.5 nm after incubation with anti-MBD2 antibody (Fig. 3C). In other words, the lack of shift in the LSPR peak demonstrated the presence of MBD2 occupied the methyl-CpG sites in the TF binding domains, inhibiting the binding of crucial TFs.

3.4. Suppression of epigenetics-mediated transcription

Small 243-bp fragments of the human p53 promoters were produced from HeLa and HEK 293 cell lines by digestion with XbaI (TCTAGA, 316/320) and BamHI (GGATCC, 73/77), then captured and enriched on the sensor surface. The 243- bp p53 promoters, containing the basic regions of promoter activity (-213 to $+1$) and a short RNA-encoding DNA region on exon 1 ($+1$ to $+30$) (243 bp), were used for monitoring of the epigenetics-mediated transcription. Positive controls were produced by methylating the 243-bp p53 promoter using the M.SssI CpG methyltransferase kit (New England Biolabs) (Supplementary Fig. S6). Real time monitoring of the epigenetics-mediated transcription on the sensor surface was sensitive, specific and used more readily than conventional methods, as the monitoring relies on steady-state measurements (Song et al., 2013; Nagy et al., 1998; Sidaway et al., 2014; Hayles et al., 2010) (Supplementary Fig. S7). The real time LSPR-peak shift was sensitive to the translocation of RNAP closer the sensor surface, due to the characteristics of δ_d. Here, we took advantage of the extraordinary surface sensitivity of LSPR, illustrated in the scheme of Fig. 1A (i), to monitor epigenetics-mediated suppression of transcription.

Once RNAP II binds into the p53 promoter and translocates downstream, the magnitude of the real time LSPR electromagnetic fields grows exponentially due to the AuNS surfaces moving closer, in the absence of MBD2 (Fig. 4A) and presence of MBD2 (Fig. 4B). Real time transcription was monitored through LSPR-peak shift. CpG methylation influences the structure, dynamics and binding

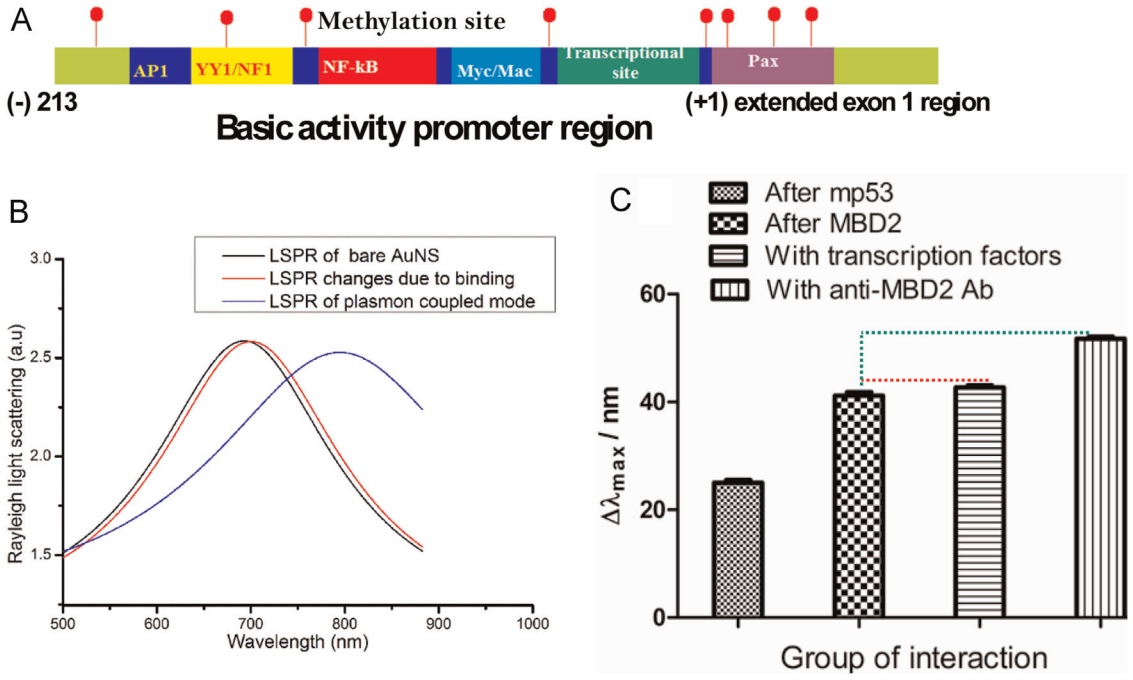

Fig. 3. Stiffness of mp53 promoter and steric competition. (A) Structure of p53 promoter and methyl-CpG sites at transcription factor binding sites. (B) Plasmonic coupling for normal p53 promoter due to its structure bending but not for mp53 promoter. The 110-nm broad peak and 6.5-nm redder shift are plasmonic coupling effect and absorbance event on AuNS surface, respectively. (C) Steric competition of MBD2 to transcription factors at their methylated DNA binding sites. The red and blue dashes indicate a comparison of LSPR shift at the step of MBD2 binding with after adding TFs (0.8 nm gap) and adding anti-MBD 2 Ab (9.5 nm), respectively. (For interpretation of the references to color in this figure legend, the reader is referred to the web version of this article.)

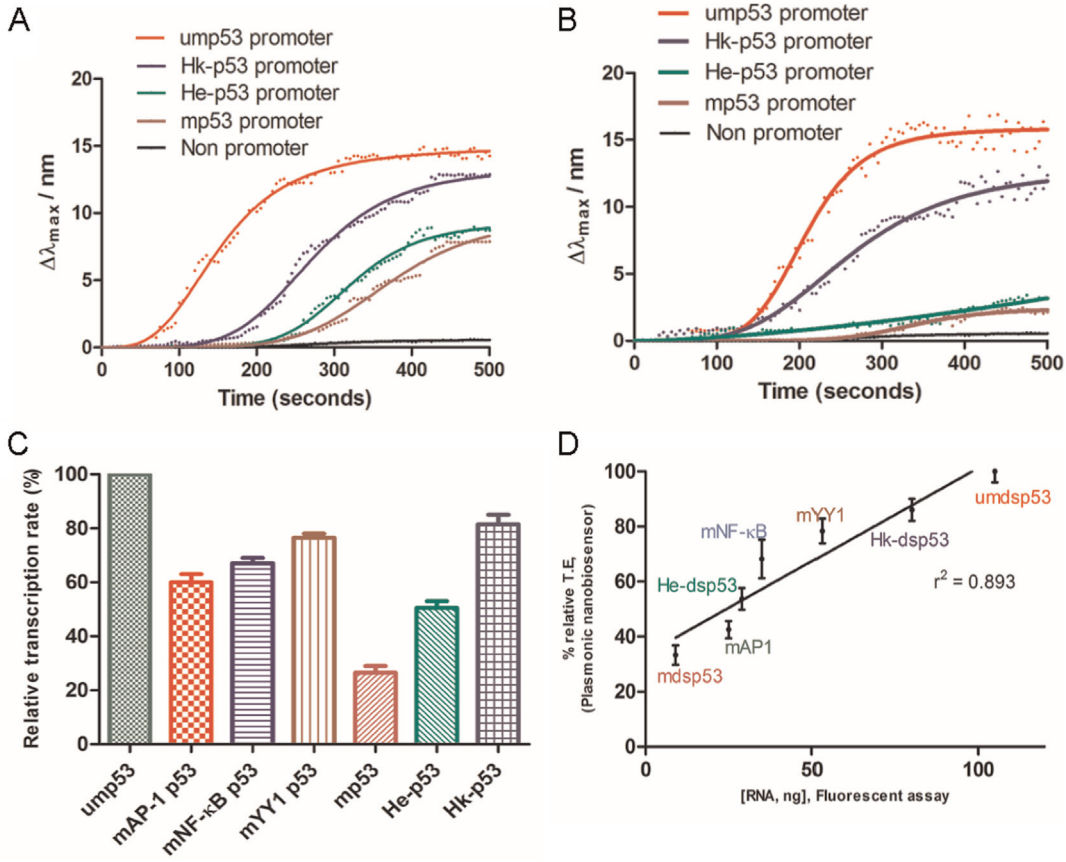

Fig. 4. Epigenetics-mediated transcription. Real-time binding and translocation of RNAP to the promoters in absence (A) and presence (B) of MBD2. The detection was done using real-time mode with 2-second interval measurement for RNA translocation closer to the surface in the surface plasmon field. (C) Relative trascription rate of each promoter in *in vitro*. (D) Degree of correlation between LSPR-shift-based. relative transcription efficiency with fluorescent assay (Qubit RNA assay, Invitrogen, USA). Using the nuclear extract from HeLa cell for the experiments.

affinity of RNAP II for the methylated DNA (Klose et al., 2005; Jones, 2012). The LSPR-peakshift-based transcription rate of RNAP II on the mp53 promoter was equal to 38.5% that of the ump53 promoter while the transcription rate of RNAP II on the He-p53 promoter was equal to 48.7% that of the Hk-p53 promoter. Moreover, the percent of transcription rates of RNAP II decreased when additional MBD2 was added. After addition, the transcription rate of RNAP II on the mp53 promoter was then equal to 4.1% that of ump53 promoter, while the transcription rate of the He-p53 promoter binding was equal to 27.4% that of the Hk-p53 promoter. The transcription rate dramatically dropped in the presence of MBD2, as it disturbs the pre-initiation complexes in the mp53 and He-p53 promoters, in comparison to the Hk-p53 and un-methylated promoters, at the beginning of each transcription cycle. Fig. 4A and B shows MBD2 binding to the methyl-CpG sites in the mp53 and He-p53 promoters, as a steric competitor. The kinetics curve can be explained by simple sterically competitive inhibition (Pommier and Marchand, 2013), disturbing formation of the transcription complex (Besmer et al., 2006).

We have shown real-time monitoring of transcription rates, which allowed calculation of the relative transcriptional efficiencies. The transcriptional efficiency of He-p53, Hk-p53, and mp53 controls were 45%, 86%, and 29%, respectively, compared to ump53 synthesized by PCR and methylated by the CpG methyltransferase kit (Fig. 4C). The sensor revealed the transcriptional efficiency of the p53 promoter in HeLa cells to be 60 times lower than that in HEK cells. The sensor-based transcriptional efficiency was correlatively analyzed with the Qubit RNA assay kit (Invitrogen, CA, USA) using a spectrofluorophotometer (Shimadzu, Kyoto, Japan). The analysis showed a correlation coefficient of $r^2=0.893$, and a standard deviation of ± 14.5 (Fig. 4D). Finally, the specificity, sensitivity, accuracy and multiplexibility of the sensor provides a platform for the measurement of epigenetic changes in native modes.

4. Conclusions

We first fabricated a novel nanoplasmonic biosensor for revealing epigenetics. The sensor can detect DNA methylation and MBD2 in HeLa and HEK cells based on their epigenetic alterations. It also revealed steric competition between MBD2 and TFs at the methylated TF binding sites. Since mp53 has decreased interaction with transcription factors, resulting from a barrier caused by the methyl groups which decreases DNA flexibility, cutting its adaptability. The sensor also detected stiffness of the mp53 promoter through the plasmon coupling mode. We also showed a kinetic model of epigenetics-mediated transcription of the promoter using the sensor. Finally, the sensor was not a simple fabrication, but also has broad applications for epigenetics. It allows measurement of the natural epigenetics of any specific gene involved in tumorigenesis. In epigenetic drug discovery, the sensor will provide a useful option for tracking activity of drug candidates.

Acknowledgments

This work was supported by the National Research Foundation of Korea (NRF) grant funded by the Korea government (Ministry of Science, ICT & Future Planning) (Grant no. NRF-2013R1A2A1A01015644/2010-0027955), and the Korea CCS R&D Center grant funded by the Korea government (Ministry of Science, ICT & Future Planning) (Grant no. 2014M1A8A1049278) of the Republic of Korea.

Appendix A. Supplementary material

Supplementary data associated with this article can be found in the online version at http://dx.doi.org/10.1016/j.bios.2014.12.015.

References

Besmer, E., Market, E., Papavasilliou, F.N., 2006. Mol. Cell Biol. 26, 4378–4385.
Brolo, A.G., 2012. Nat. Photonics 6, 709–713.
Brown, S.E., Fraga, M.F., Weaver, I.C., Berdasco, M., Szyf, M., 2007. Epigenetics 2, 54–65.
Browning, D., Savery, N., Kolb, A., Busby, S., 2009. Methods Mol. Biol. 543, 369–387.
De, A., Souchelnytskyi, S., Berg, A., v.d., Carlen, E.T., 2013. ACS. Appl. Mater. Interfaces 5, 4607–4612.
Deaton, A.M., Bird, A., 2011. Genes Dev. 25, 1010–1022.
Egger, G., Liang, G., Aparicio, A., Jones, P.A., 2004. Nature 429, 457–463.
Hayles, B., Yellaboina, S., Wang, D., 2010. PLos One 5, e9908. http://dx.doi.org/10.1371/journal.pone.0009908.
Hu, J., Zhang., C.Y., 2012. Biosens. Bioelectron 15, 451–457.
Jolma, A., Yan, J., Whitington, T., Toivonen, J., Nitta, K.R., Rastas, P., Morgunova, E., Enge, M., Taipale, M.G., Palin, K., Vaquerizas, J.M., Vincentelli, R., Luscombe, N. M., Hughes, T.R., Lemaire, P., Ukkonen, E., Kivioja, T.J., 2013. Cell 152, 327–339.
Jones, P.A., 2012. Nature Rev. Genet. 13, 484–492.
Klose, R.J., Sarraf, S.A., Schmiedeberg, L., McDermott, S.M., Stancheva, I., Bird, A.P., 2005. Mol. Cell 19, 667–678.
Kugel, J.F., Goodrich, J.A., 1998. Proc. Natl. Acad. Sci. USA 95, 9232–9237.
Kuznetsov, S.V., Sugimura, S., Vivas, P., Crothers, D.M., Ansari, A., 2006. Proc. Natl. Acad. Sci. USA 103, 18515–18520.
Lange, H., Juárez, B.H., Richter, M., Bastús, N.G., Weller, H., Thomsen, C., Klitzing, Rv., Knorr, A., 2012. Langmuir 28, 8826–8866.
Nagy, J.L., Leisztner, L., Hangos, K.M., 1998. J. Automat. Chem 10, 101–105.
Nehl, C.L., Liao, H., Hafner, J.H., 2006. Nano Lett. 6, 683–688.
Nielsen, P.E., Egholm, M., Berg, R.H., Buchardt, O., 1991. Science 254, 1497–1500.
Ng, H.H., Zhang, Y., Hendrich, B., Johnson, C.A., Turner, B.M., Erdjument-Bromage, H., Tempst, P., Reinberg, D., Bird, A., 1999. Nature Genet. 23, 58–61.
Nguyen, A.H., Sim, S.J., 2014. Biosens. Bioelectron , http://dx.doi.org/10.1016/j.bios.2014.09.003.
Oshiro, M.M., Watts, G.S., Wozniak, R.J., Junk, D.J., Monoz-Rodriguez, I.L., Domann, F.E., Futscher, B.W., 2003. Oncogene 22, 3624–3634.
Penagarikano, O., Mulle, J.G., Warren, S.T., 2007. Annu. Rev. Genomics Hum. Genet. 8, 109–129.
Pogribny, I.P., Pogribna, M., Christman, J.K., James, S.J., 2000. Cancer Res. 60, 588–594.
Pommier, Y., Marchand, C., 2013. Nat. Rev. Drug Discov. 11, 25–36.
Reinhard, B.M., Agarwal, H., Alivisatos, A.P., Liphardr, L., 2005. Nano Lett. 5, 2246–2252.
Reinhard, B.M., Sheikholeslami, S., Mastroianni, A., Alivisatos, A.P., Liphardt, J., 2007. Proc. Natl. Acad. Sci. USA 104, 2667–2672.
Ringe, E., Langille, M.K., Sohn, K., Zhang, J., Huang, J., Mirkin, C.A., Van Duyne, R.P., Marks, L.D., 2012. J. Phys. Chem. Lett. 3, 1479–1483.
Robertson, K.D., 2002. Oncogene 21, 5361–5379.
Rodríguez-Lorenzo, L., de la Rica, R., Álvarez-Puebla, R.A., Liz-Marzán, L.M., Stevens, M.M., 2012. Nat. Mater. 11, 604–607.
Shim, J., Humphreys, G.I., Venkatesan, B.M., Munz, J.M., Zou, X., Sathe, C., Schulten, K., Kosari, F., Nardulli, A.M., Vasmatzis, G., Bashir, R., 2012. Sci. Rep. 3, 1389. http://dx.doi.org/10.1038/srep01389.
Sidaway, L.K., Costa, M.J., Rand, D.A., Finkenstadt, B., Penfield, S., 2014. Genome Biol. 15, R45. http://dx.doi.org/10.1186/gb-2014-15-3-r45.
Song, M.S., Choi, S.P., Lee, J., Kwon, Y.J., Sim, S.J., 2013. Adv. Mater. 25, 1265–1269.
Sonnichsen, C., Reinhard, B.M., Liphardt, J., Alivisatos, A.P., 2005. Nat. Biotechnol. 23, 741–745.
Stains, C.J., Furman, J.L., Segal, D.J., Ghosh, I., 2006. J. Am. Chem. Soc. 30, 9761–9765.
Tsunoda, T., Takagi, T., 1999. Bioinformatics 15, 622–630.
Wang, Y., Zhang, C.H., Tang, L.J., Jiang, J.H., 2012. Anal. Chem. 16, 8602–8606.
Zhang, J., Xing, B., Song, J., Zhang, F., Nie, C., Jiao, L., Liu, L., Lv, F., Wang, S., 2014. Anal. Chem. 86, 346–350.